Chaos, Solitons and Fractals 164 (2022) 112735

Contents lists available at ScienceDirect

Chaos, Solitons and Fractals

journal homepage: www.elsevier.com/locate/chaos

Multilayer networks with higher-order interaction reveal the impact of collective behavior on epidemic dynamics

Jinming Wan [a], Genki Ichinose [b], Michael Small [c,d], Hiroki Sayama [a], Yamir Moreno [e,f,g], Changqing Cheng [a,h,*]

[a] Department of Systems Science and Industrial Engineering, State University of New York, Binghamton, NY 13902, United States of America
[b] Department of Mathematical and Systems Engineering, Shizuoka University, 3-5-1 Johoku, Naka-ku, Hamamatsu 432-8561, Japan
[c] Complex Systems Group, Department of Mathematics and Statistics, The University of Western Australia, Crawley, WA 6009, Australia
[d] Mineral Resources, CSIRO, Kensington, WA 6151, Australia
[e] Institute for Biocomputation and Physics of Complex Systems, University of Zaragoza, 50018 Zaragoza, Spain
[f] Department of Theoretical Physics, University of Zaragoza, 50009 Zaragoza, Spain
[g] CENTAI Institute, Torino, 10138, Italy
[h] ISI Foundation, Torino, 10126, Italy

ARTICLE INFO

Keywords:
Multilayer networks
Collective behavior
Contagion dynamics
Simplicial complex

ABSTRACT

The ongoing COVID-19 pandemic has inflicted tremendous economic and societal losses. In the absence of pharmaceutical interventions, the population behavioral response, including situational awareness and adherence to non-pharmaceutical intervention policies, has a significant impact on contagion dynamics. Game-theoretic models have been used to reproduce the concurrent evolution of behavioral responses and disease contagion, and social networks are critical platforms on which behavior imitation between social contacts, even dispersed in distant communities, takes place. Such joint contagion dynamics has not been sufficiently explored, which poses a challenge for policies aimed at containing the infection. In this study, we present a multi-layer network model to study contagion dynamics and behavioral adaptation. It comprises two physical layers that mimic the two solitary communities, and one social layer that encapsulates the social influence of agents from these two communities. Moreover, we adopt high-order interactions in the form of simplicial complexes on the social influence layer to delineate the behavior imitation of individual agents. This model offers a novel platform to articulate the interaction between physically isolated communities and the ensuing coevolution of behavioral change and spreading dynamics. The analytical insights harnessed therefrom provide compelling guidelines on coordinated policy design to enhance the preparedness for future pandemics.

1. Introduction

In the absence of pharmaceutical interventions, situational awareness and collective adoption of protective behaviors are pivotal to combat spreadout of infectious diseases, as demonstrated by the ongoing COVID-19 pandemic and the flare-up or resurgent outbreaks around the world. The integration of awareness into mathematical models, mainly through variants of susceptible-infectious-recovered (SIR) models, has been widely investigated since the onset of COVID-19 [1]. Most of these models merely capture oversimplified behaviors (e.g., social distancing or not) and fail to capture the sophisticated mechanisms underlying behavioral responses, including the individual perception of infection risk and bounded rationality, government mandate, socioeconomic cost and fatigue on adherence to containment policies, as well as social influence [2–5]. The interplay between the collective behavioral response of the population and the contagion dynamics has a significant bearing on the epidemic evolution.

Game-theoretic models explicitly account for behavioral adaptation and the connection with epidemic spreading [6], mostly with a separation of time scales between the spreading dynamics and behavioral response [7–10]. For instance, behavioral changes only occur at the beginning of each time period or happen at a much lower frequency. Such a time-scale separation does not capture the realism of behavioral responses. Inspired by [11], we study the coevolution of the spreading

* Corresponding author at: Department of Systems Science and Industrial Engineering, State University of New York, Binghamton, NY 13902, United States of America.
E-mail address: ccheng@binghamton.edu (C. Cheng).

https://doi.org/10.1016/j.chaos.2022.112735
Received 27 August 2022; Accepted 20 September 2022
Available online 14 October 2022

dynamics and behavioral adaptation under the same time scale and investigate the decision-making process under the influence of risk perception, behavioral change costs, compliance fatigue, social influence, as well as bounded rationality [12]. As behavior dynamics has been recognized as one driving force behind resurgent outbreaks of COVID-19, there is a pressing demand for a paradigm shift from purely rational and reactive behavior modeling to a more comprehensive response computational framework that can predict the epidemic evolution and provide guidance on intervention policy design.

Network models have been widely deployed to describe agent interactions. For instance, a single-layer network was suggested in [13] to incorporate agent behavior to extend the conventional susceptible-exposed-infectious-recovered (SEIR) model. The decision of each agent to take a certain behavioral response is modeled via an evolutionary game model, considering the underlying cost. Ye et al. [11] instead suggested a two-layer network to study the interplay between agent behavior from a social layer and the spreading dynamics on a physical layer. Particularly, as we have observed during the COVID-19 pandemic, social media play a vital role in reshaping our perception towards the risk of infection and in transforming behavioral responses. Nonetheless, most existing works only study the interplay between epidemic dynamics and behavior responses for the population that resides in the same physical community. It has been reported that contact patterns of residents in one region could be substantially affected by the policies and behavioral responses in other distant regions [14]. Or in other words, we imitate behavioral responses of our social contacts even if we are located in distant communities. Such a "spillover" effect could crimp the effectiveness of intervention policies, and it has not been systematically investigated. On the other hand, numerous behavioral models [6], [15,16] have been proposed to quantify how human behaviors adapt and affect the transmission of contagious diseases assuming pairwise interactions between agents. It is noted, however, that this pairwise interaction assumption may fail to represent more realistic behavioral responses [17]. Instead, a higher-order interaction among the population has been suggested for behavioral adaptation on social networks. Recent studies also underscore that the presence of higher-order interactions substantially sways the dynamics of networked systems, from diffusion and synchronization to social and evolutionary processes, possibly leading to the emergence of sophisticated collective phenomena [17–19].

To account for such phenomena, we propose a three-layer network platform to study the interplay between behavioral response and contagion process in two distant communities. These two communities interact via a common social network. A simplicial complex is adopted to model the high-order interactions on the social layer, and a game-theoretic model is then utilized to elucidate the behavioral change of agents. This theoretic model could help harvest policy-relevant insights into the course of contagion spreading dynamics.

It is noteworthy to highlight that our model is not intended to replicate real curves because we are more interested in specific system reactions, such as behavioral responses and changes. Generally, most results caused by diverse behaviors are inadequate data to characterize behaviors. If we fully focus on the result and ignore the mechanisms underlying these behaviors, the result will no longer be precise when the behavioral responses are changed. Currently, most COVID-19 predictions are inaccuracy and their prediction curve are too smooth to be true because the practical curves are oscillations. Thus, we do not target reproducing real results or curves but focus on analytical insights.

2. Background

Modeling and simulation of epidemics abound in the literature. Such models provide critical insight into the spreading dynamics and are imperative in the optimal design of knowledge-informed intervention policies. Compartment models and their variants (e.g., SIR [20]) are the most popular approaches in epidemic modeling. They divide the population into different compartments and use ordinary differential equations to capture the dynamic evolution of population flow across the different compartments. The SEIR variant includes an exposed compartment between the susceptible and infectious to account for the incubation period of the disease, and it has been used to predict COVID-19 infection and hospital resource shortage at the state-level in the U.S. [21] and other countries. However, a classical compartmental model typically relies on a key assumption of population homogeneity in a certain region or community of interest, and each compartment represents an aggregate of indistinguishable individuals. This is not realistic to unveil the critical distinctions pertaining to epidemic dynamics. Admittedly, recent studies have set forth strong evidence of spatial heterogeneity and disparities in COVID-19 transmissions [22,23]. Socioeconomic, cultural, and environmental factors, which differ across geographic communities, could substantially affect human behavior, and consequently, the spread of COVID-19. Thus, accurate modeling requires a more refined approach to address the heterogeneity of populations. Prem et al. [24] proposed an age-structured SEIR model and divided the whole population into 16 age groups to assess the effectiveness of physical distancing measures in containing COVID-19 in Wuhan, China. Kucharski et al. [25] investigated a stochastic SEIR model with random contact rates to forecast the case count of COVID-19 in Wuhan and other cities. In the metapopulation SEIR model, a certain geographic area is divided into multiple distinct communities, each with unique geographic and demographic features. A local SEIR model is then imposed for each region, and those local SEIR models are coupled together to quantify the daily transmission within and between the regions. Tran-Thi et al. [26] proposed a stochastic SEIR metapopulation model that included both population migration and environmental transmission (seasonal average contact rate) for the spread of infectious diseases. Similarly, Venkatramanan et al. [27] integrated short- and long-range mobility patterns in a SEIR metapopulation model to study the contagion of seasonal influenza. Brockmann and Helbing [28] replaced the conventional geographic distance with effective distance derived from the mobility network and built a simplified and homogeneous metapopulation SIR model to predict arrival times of infection peaks. Acknowledging that epidemiological parameters are often hard to calibrate and typically associated with huge uncertainty, which may render the model useless, this simplified and homogenous modeling approach [28] relies on only a small fraction of transport connections with fewer parameters to fit.

Yet, the resurgent outbreaks and flare-up of case counts around the world suggest that population behavior plays a critical role in shaping the spreading dynamics. For example, Rădulescu et al. [29] incorporated different population behaviors (social distancing, mobility restrictions, and lockdowns) into a conventional SEIR model to simulate the epidemic dynamics. The results indicated that whereas social distancing is effective in flattening the contagion curve, it cannot completely rule out resurgent outbreaks. Weitz et al. [30] combined a SEIR model with fatality-driven awareness and reported that the situational awareness leads to asymmetric epidemic curves with lagged oscillations. Lockdown fatigue was also considered to examine the impact from premature relaxation of mobility reductions on the resurgence of outbreaks [30]. In a similar vein, Johnston and Pell [31] proposed a behavior-perception SEIR model that incorporates fear of infection and frustration of social distancing to study the second-wave of COVID-19.

We also note that the heterogeneity of individual behavioral responses to the government mandate has complicated the effort to contain the spread. Scabin et al. developed a multi-layer network to consider social activities in different scenarios, including home, workplace, transportation, and school, and the impact on a seven-state compartment model [32]. Chinazzi et al. [33] combined the SEIR model and metapopulation network with real-world airline transportation data to predict the infection rates in major cities in China. Similarly, Wu et al. [34] applied a SEIR model to a transportation network that connects spatially disjoint regions to predict the spread of

COVID-19 in China. Cui et al. [35] applied a SEIR model on different Barabási-Albert (BA) [36] networks to simulate transmission of COVID-19 with different physical contacts, subject to the testing procedure set by the government. Considering the inflows and outflows of interstate travel, a mobility network-based SEIR model was developed to project state-wise COVID-19 infection in the U.S. and to assess the impact of non-pharmaceutical intervention policies at the state level [21]. In [37], a metapopulation SEIR model was overlaid on a mobility network, which governs how populations from different social groups interact as they visit points of interest. Similarly, Meloni et al. [38] implemented a metapopulation model into a mobility network but considered various self-initiated behavioral responses for individual's mobility pattern. The authors analyzed the behavioral responses in both synthetic and data-driven scenarios and indicated that behavioral responses with the goal of limiting and decreasing the pandemic may have the exact opposite impact.

Social networks play an increasingly important role in shaping our daily behaviors [15], including our attitude and response to the prevalence of infections. Alvarez-Zuzek et al. [39] developed a two-layer network to evaluate the influence of social opinion in vaccination on epidemic spreading. Similar studies [40–43] also implied that agent interaction on the social layer has a tremendous influence on the incidence of infection and the outbreak of epidemics on the physical layer. In [44], the authors claimed that diffusion of negative or positive opinion towards the infection can lead to risk-taking or risk-averse behaviors, respectively, which further elevate or suppress the prevalence rate. Other factors and their influence on the behavioral response have also been studied, including risk perception (awareness) [7,43], compliance cost [45], bounded rationality [12], and non-pharmaceutical intervention policy (containment measure) [46–48].

In these modeling studies, the population resides in the same physical and virtual communities. Their perception of infection risk and opinion formed from their social interactions reshape their behavioral response in the physical community. In reality, we also interact with social contacts in disjoint communities and may imitate their response to the infection. This cannot be elucidated via the above-mentioned network modeling approaches. In particular, pair-wise interactions between agents on the social network are widely used, which are oftentimes not sufficient to account for the rich collective dynamics underneath a variety of social imitation phenomena, including opinion formation and behavioral adaptation. Indeed, pairwise links do not operate alone on the social layer. Rather, they are usually reinforced by group pressure. It has been suggested that complex mechanisms of higher-order influence and reinforcement are at play and responsible for a variety of emergent collective behaviors [19]. In this investigation, we describe such higher-order interactions on the social network with simplicial complexes and study the social influence on infection dynamics in two distant physical communities.

3. Model

We present a multilayer network platform to elucidate how the collective behavior of individual agents affects the contagion dynamics on disjoint physical communities. This platform comprises two physical layers that represent two isolated communities A and B, on top of which a networked SEIR model is implemented to capture the disease spreading dynamics. Here, for simplicity, we construct the communities A and B as Barabási-Albert (BA) networks, since many realistic networks follow the preferential attachment principle [36]. The physical networks of communities A and B have N_a and N_b nodes or agents, respectively. In essence, starting with an initial network G_0 of N_0 connected nodes, new nodes are attached to $m < N_0$ original ones to form new edges according to the preferential attachment principle, i.e., with a probability proportional to the degree of existing nodes.

Agents from both communities A and B collectively define a social community C that accommodates social interactions, thus the size $N_c = N_a + N_b$ (see Fig. 1). These two physical layers have time-varying undirected links, which symbolize the physical contacts or the avenue for disease transmission [49]. Each agent adjusts their risk-taking or risk-averse behaviors as they parse information regarding the global prevalence of the contagion and the response of their neighbors on the social layer. Therefore, the two distant communities could still affect each other regarding the spreading dynamics indirectly via the social network, even without human mobility in between. This mimics how we perceive information from social media and adapt our behaviors accordingly.

We define two utility functions π_a^i and π_r^i to characterize the payoff for risk-averse and risk-taking behaviors of agent i, which hinges on the effective intervention policy $\delta(t)$, imitation of social influence $\omega_i(t)$, compliance cost $\varepsilon_i(t)$ (e.g., economic cost, mental stress, and physical fatigue), and the community's risk perception $\eta(t)$ [11].

$$\pi_a^i(t) = \omega_i(t) + \eta(t) - \varepsilon_i(t) \tag{1a}$$

$$\pi_r^i(t) = -\delta(t) - \omega_i(t) \tag{1b}$$

With a large π_a^i, agent i has a strong sense of situational awareness and tends to be risk-averse, disregarding the effective intervention policy δ. It is further assumed that conservative agents are sensitive to risk perception $\eta(t)$ and compliance cost $\varepsilon_i(t)$, as displayed in Eq. (1a). Conversely, a large π_r^i indicates that agent i is risk-prone. The risk-taking agents generally ignore the risk perception $\eta(t)$ and compliance cost $\varepsilon_i(t)$. They instead subject their behaviors to government regulations. $\omega_i(t)$ prescribes the social influence on agent i resulting from imitating the behaviors of social contacts. Positive $\omega_i(t)$ indicates imitation of protective behaviors from neighbors, thus boosting $\pi_a^i(t)$; negative $\omega_i(t)$ implies imitation of risk-taking responses, elevating $\pi_r^i(t)$. Following this, we construct a Markov model to characterize the time-dependent behavioral adaption via behavior quotient (BQ) $x_i(t+1)$ of agent i at time stamp $t+1$ with bounded rationality assumption:

$$x_i(t+1) = \frac{e^{\sigma\pi_a^i(t)} - e^{\sigma\pi_r^i(t)}}{e^{\sigma\pi_a^i(t)} + e^{\sigma\pi_r^i(t)}}, \tag{2}$$

where $\sigma > 0$ is a rational scale in the decision-making process. A finite constant σ is assumed for all agents with bounded rationality. As a side note, the two extreme cases of $\sigma \to \infty$ and $\sigma = 0$ indicate fully rational and fully irrational behaviors, respectively. The BQ $x_i(t) \in (-1, 1)$ is a continuous variable capturing the effective behavioral response of agent i: if $x_i(t) > 0$, agent i avoids risk and takes protective behavior; for $x_i(t) = 0$, agent i is risk-neutral; if $x_i(t) < 0$, risky behavior is in favor, which could potentially boost the probability of infection. It is noteworthy that the formulation of BQ $x_i(t)$ is a significant departure from the model proposed in [11], in that each agent mimics both risk-averse and risk-taking behaviors. The public weighs the trade-off to adjust their behavioral response, considering the behavior of their social contacts, risk perception, government intervention policy, and compliance cost.

3.1. Imitation of social behavior

On the social influence layer, we define an imitation function $\omega_i(t)$ to characterize how agent i imitates the behaviors of their social contacts. The simplicial complex has been extensively used to reveal such higher-order interactions: the behavioral imitation occurs with nonlinear reinforcement characterized by the simplex dimension, rather than bilinearly depending on the number of connecting nodes and their behaviors. Formally, a simplex of dimension d or d-simplex is a collection of $d+1$ vertices $\sigma_d = [j_0, j_1, \ldots, j_d]$, and any subset $\sigma_{d'}$ ($d' \leq d$) of σ_d is its sub-simplex or d'-face [17]. That said, σ_d subsumes all subset simplices of dimension $d-1$, and so on recursively. The vertices are called 0-simplices, the edges the 1-simplices and the full triangles the 2-simplices. The collection of simplices and all the sub-simplices or faces

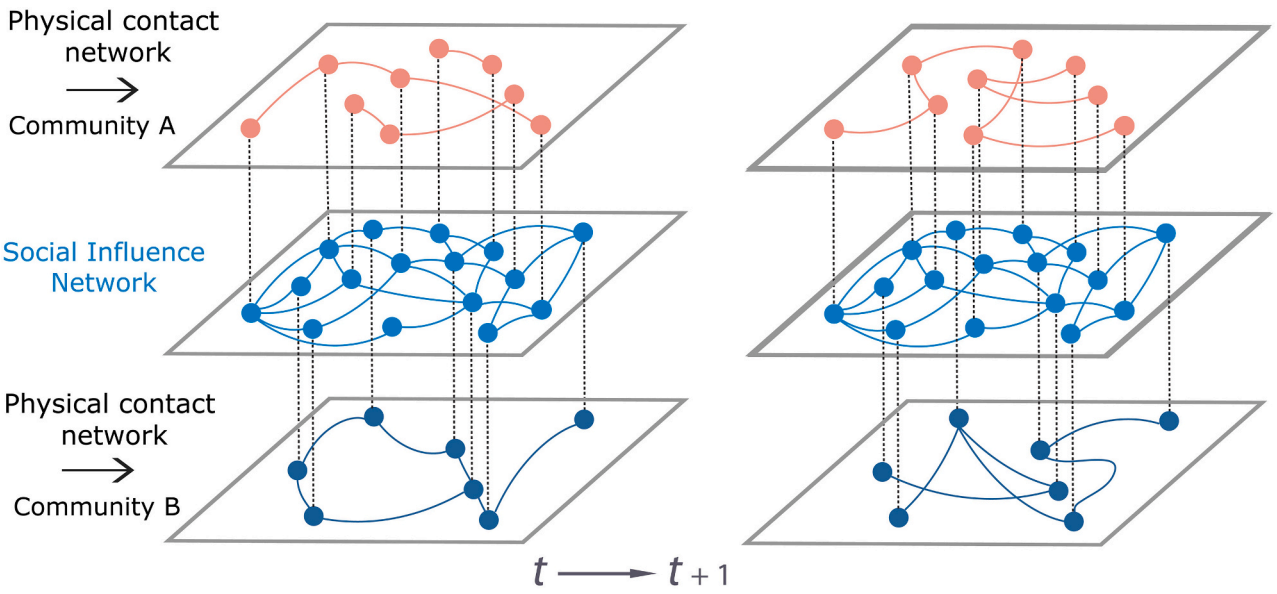

Fig. 1. Illustration of the 3-layer network platform as time evolves: the upper layer and lower layer represent the two physical contact networks or communities *A* and B; the middle layer represents the social influence network.

defines a simplicial complex. As illustrated in Fig. 2(b), the agent i (the orange node) interacts with a set of social contacts j_1, j_2 and j_3 via a simplicial 2-simplex, which contains a 1-simplex (e.g., pairwise link of $[i, j_1]$)and a 2-simplex (the full triangle $[i, j_2, j_3]$). Conversely, Fig. 2(a) illustrates a simplicial 1-complex with only the pairwise interactions. The imitation of social behavior, indexed by ω_i, is induced on the simplicial complex. For computational easiness, we only consider the simplicial complex up to dimension 3 in this study.

The enhancement effect for collective interaction of a d'-simplex is given as $\theta_{d'} = (1+\rho_{d'})^{\lambda_{d'}}$, where $\rho_{d'}$ is the proportion of number counts of d'-simplices in the simplicial 3-complex. $\lambda_{d'} = \left(\frac{d'+1}{3}\right)$ underscores the influence of high-order interactions. $\lambda_{d'} = 0$ for $d' < 2$, $\lambda_2 = \left(\frac{2+1}{3}\right) = 1$, and $\lambda_3 = \left(\frac{3+1}{3}\right) = 4$. In the illustrative example depicted in Fig. 2 (c), a simplicial 3-complex contains three 1-simplices, four 2-simplices, and three 3-simplices, thus $\rho_1 = \rho_3 = \frac{3}{10}$, $\rho_2 = \frac{4}{10}$. Correspondingly, the enhancement coefficient for pairwise interaction is fixed as $\theta_1 = 1$ with $\lambda_1 = 0$. Therefore, the imitation of social behavior function for agent i at time t can be represented as:

$$\omega_i(t) = \xi \frac{\theta_1 \sum_{v=1}^{n_{i1}} \bar{x}_v^1 + \theta_2 \sum_{v=1}^{n_{i2}} \bar{x}_v^2 + \theta_3 \sum_{v=1}^{n_{i3}} \bar{x}_v^3}{n_i}, \tag{3}$$

where ξ is the imitation factor that scales the influence of imitation behavior in utility functions π_a^i and π_r^i, n_{i1} is the number of 1-faces, n_{i2} is the number of 2-faces, and n_{i3} is the number of 3-faces associated with agent i. Variables $\bar{x}_v^1$, $\bar{x}_v^2$, and $\bar{x}_v^3$ represent the average BQ of the v^{th}face with orders 1, 2, and 3 respectively. The 1-face is included not only in the 1-simplex but also in the 2-simplex and 3-simplex. Each 1-face contains one neighboring agent for agent i with the average BQ $\bar{x}_v^1(t)$. Here $\bar{x}_v^1(t) = x_{j_v}(t)$, $v = 1, \ldots, n_{i1} = 20$ as shown in Fig. 2(c). Similarly, the 2-face is included not only in the 2-simplex but also in the 3-simplex, and 2-face contains two neighboring agents with average BQ $\bar{x}_v^2(t)$. There are thirteen 2-faces for agent i in Fig. 2(c), which are $\bar{x}_1^2(t) = \frac{x_{j_1}(t)+x_{j_2}(t)}{2}$, $\bar{x}_2^2(t) = \frac{x_{j_1}(t)+x_{j_3}(t)}{2}$, $\bar{x}_3^2(t) = \frac{x_{j_2}(t)+x_{j_3}(t)}{2}$, $\bar{x}_4^2(t) = \frac{x_{j_4}(t)+x_{j_5}(t)}{2}$, $\bar{x}_5^2(t) = \frac{x_{j_8}(t)+x_{j_9}(t)}{2}$, $\bar{x}_6^2(t) = \frac{x_{j_{11}}(t)+x_{j_{12}}(t)}{2}$, $\bar{x}_7^2(t) = \frac{x_{j_{11}}(t)+x_{j_{13}}(t)}{2}$, $\bar{x}_8^2(t) = \frac{x_{j_{12}}(t)+x_{j_{13}}(t)}{2}$, $\bar{x}_9^2(t) = \frac{x_{j_{14}}(t)+x_{j_{15}}(t)}{2}$, $\bar{x}_{10}^2(t) = \frac{x_{j_{16}}(t)+x_{j_{17}}(t)}{2}$, $\bar{x}_{11}^2(t) = \frac{x_{j_{16}}(t)+x_{j_{18}}(t)}{2}$, $\bar{x}_{12}^2(t) = \frac{x_{j_{17}}(t)+x_{j_{18}}(t)}{2}$, and $\bar{x}_{13}^2(t) = \frac{x_{j_{19}}(t)+x_{j_{20}}(t)}{2}$. Lastly, the 3-face is only included in the 3-simplex, and there are three 3-faces in the illustrative example in Fig. 2(c). The average BQ $\bar{x}_1^3(t) = \frac{x_{j_1}(t)+x_{j_2}(t)+x_{j_3}(t)}{3}$, $\bar{x}_2^3(t) =$

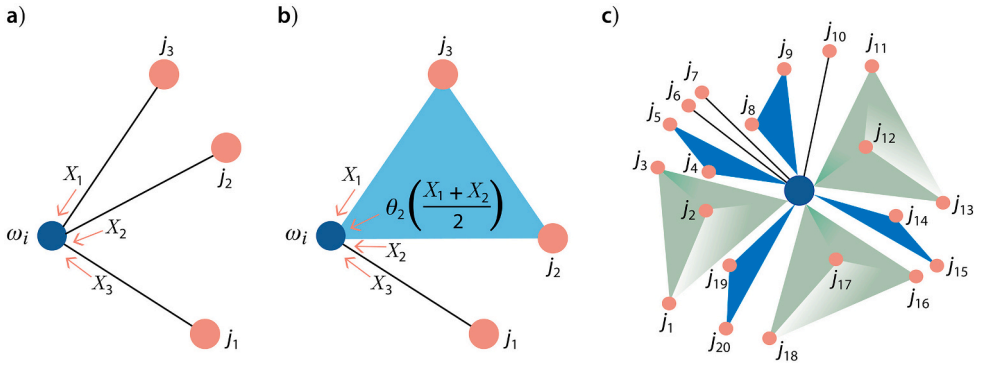

Fig. 2. Illustration of different interactions in the network for agent *i*: (a) only pairwise interactions; (b) simplical 2-complex, including the pairwise and full-triangle interactions; (c) a simplicial 3-complex with three 3-simplices, four 2-simplices, and three 1-simplices.

$\frac{x_{j11}(t)+x_{j12}(t)+x_{j13}(t)}{3}$, and $\bar{x}_3^3(t) = \frac{x_{j16}(t)+x_{j17}(t)+x_{j18}(t)}{3}$.

3.2. Risk perception

The risk perception reflects how the public perceives the disease prevalence z, the fraction of the population that is infected (exposed and infectious) [50]. A power function for risk perception, $z(t) \in [0,1]$, has been suggested in [11]:

$$\eta(t) = kz(t)^u, \tag{4}$$

where $k > 0$ is the scaling factor and the risk index $u > 0$ captures the population attitude towards the prevalence or the risk. Since $z \in (0,1)$, $u > 1$ indicates that the population discounts the infection risk, and $u < 1$ implies that the public tends to overrate the underlying risk.

3.3. Government intervention policies

To contain the spreading of infection, the government enacts non-pharmaceutical interventions, such as social distancing, face mask requirement, and lockdowns. $p(t) > 0$ quantifies the strength of such policies at time t, and the policy is adjusted periodically (e.g., every 10 time steps) for each community according to the average prevalence $\bar{z}(t^*)$ of the previous time interval $T \in [t^* - 10, t^* - 1]$, where $t^* = 10 \times \lfloor \frac{t}{10} \rfloor$ and $\lfloor \bullet \rfloor$ is a floor function. Remarkably, public compliance with social restrictions diminishes as fatigue sets in. To account for the "lockdown fatigue", a fatigue function $\psi(t) = e^{-\left(\frac{t}{\mu}\right)}$ is introduced to portray the diminishing public compliance to the intervention policy as time elapses, regulated by the complying factor μ. Thus, the effective intervention policy δ is given as:

$$\delta(t) = \psi(t)p(t), \tag{5a}$$

$$p(t) = \begin{cases} 0.8, & \bar{z}(t^*) \rangle 0.1 \\ 0.5, & 0.05 \le \bar{z}(t^*) \le 0.1 \\ 0.3, & 0.03 \le \bar{z}(t^*) \langle 0.1 \\ 0.0, & \bar{z}(t^*) \langle 0.03 \end{cases}, \tag{5b}$$

Here, the values of $p(t)$ are set arbitrarily, and we do not seek to find the optimal intervention policy. Different evolution trajectory of the infection of the two different communities causes different intervention policies $p(t)$, as shown in Eq. (5b). We name this as an adjustable policy, in comparison to the rigid policy to be discussed in Section 4.

3.4. Compliance cost

Studies on historical contagion indicates that adherence to government mandate is crucial to slowing the spread of the pandemic [14]. The compliance cost $\varepsilon_i(t)$ symbolizes the cost of abiding by government policies, and it hinders the agent from taking protective behaviors (e.g., shelter-at-home and wearing face masks). The compliance cost $\varepsilon_i(t)$ comprises two components: the immediate cost $c \ge 0$, e.g., basic sanitization cost and psychological frustration, and cumulative protective cost.

$$\varepsilon_i(t) = c + \sum_{\tau=1}^{t} a^{t-\tau}(\varphi[x_i(\tau) - 0.2]^+) \tag{6}$$

$a \in [0,1]$ is the cumulative factor representing how the past protective behaviors affect the current compliance cost. As agents respond to the infection in a different way, the cumulative cost hinges on each BQ $x(t)$. $a = 0$ implies a memoryless protective cost structure, such that the protective action course in the history does not affect the current compliance cost. Cost scaling φ indicates the cost associated with the protective behaviors. $[x_i(\tau) - 0.2]^+ = max(0, x_i(\tau) - 0.2)$ represents that the BQ <0.2 will not incur a cost at time τ.

3.5. Transition probability

On the two physical contact layers (communities A and B), each agent i is in one of 4 possible states $h_i(t) = \{S, E, I, R\}$ at any time t. The infectious (I) spreads the disease to their susceptible (S) neighbors, who then become exposed (E) with a probability $P(h_i(t+1) = E \,|h_i(t) = S)$:

$$P(h_i(t+1) = E \,|h_i(t) = S) = \frac{1 - x_i(t)}{2} \times \left(1 - (1-\beta)^{N_i(t)}\right), \tag{7}$$

where β is the infection rate when the susceptible agent i contacts infectious neighbors. $N_i(t)$ is the number of infectious neighbors for agent i at time t, and it is time-varying because of the change of agents' states. The expression $\frac{1-x_i(t)}{2} \in (0,1)$ symbolizes the effective disease transmission, citing variation of BQ $x_i(t)$. When $x_i(t) = 1$, agent i refrains from taking any risk, and $x_i(t) = -1$ implies that agent i completely ignores the infection risk. The exposed (E) transitions to the infectious (I) with a probability $P(h_i(t) = I \,|h_i(t_E) = E)$:

$$P(h_i(t) = I \,|h_i(t_E) = E) = 1 - e^{-\alpha(t - t_E)}, \tag{8}$$

where t_E is the time at which agent i becomes exposed (E). This transition occurs at an exponential rate α, or equivalently with an average latent period of $1/\alpha$. In a similar vein, the infectious (I) recovers with a probability $P(h_i(t) = R \,|h_i(t_I) = I)$:

$$P(h_i(t) = R \,|h_i(t_I) = I) = 1 - e^{-\gamma(t - t_I)}, \tag{9}$$

where t_I is the time at which agent i becomes infectious (I). The recovery process occurs at an exponential rate γ, or equivalently with an average recovery period of $1/\gamma$.

4. Numerical results

We utilize the Facebook social network dataset from Network Repository (NR) [51] for the social influence layer, which includes 10,004 individual Facebook users or nodes. We construct a simplicial 3-complex for each agent at each time t by randomly selecting a different number of neighbors (from 1 to 3) to formulate different order simplices. We generate an Erdös-Rényi (ER) random network as the initial network G_0 with size $N_0 = 1000$ and the probability of node connection $C_0 = 0.1$ to construct two BA networks to represent the communities A (the first physical contact layer in our multilayer network) and B (the second physical contact layer) of equal size $N_a = N_b = 5002$ but with disparate density of links. The densely connected network symbolizes the urban area, denoted as community A: each of the new coming nodes will connect to $m_a = 250$ nodes to extend the initial network. The sparsely connected network is analogous to the rural area, denoted as community B: each new coming node will be connected to only $m_b = 50$ existing nodes. The connectivity of these two BA networks represents the maximal physical contacts for each agent throughout the epidemic process. As time evolves, a random set of edges from this connectivity will be chosen for each agent to form the time-varying network. This does not preclude other temporal formation mechanisms [11]. We stress that whereas some epidemic models can reproduce key features of the spreading dynamics, the abundance of mutually incompatible models suggest that there is still substantial uncertainty in data collection and model parameterization, as well as a lack of fundamental understanding of the observed spatiotemporal dynamics [28]. Thus, we do not aim to replicate the infection curve in any particular regions. Rather, we parameterize the model to reveal the general impact of the social interplay on the infection dynamics.

We implement the SEIR compartment model previously described on the two physical layers (the communities A and B), which possess the same key parameters for the COVID-19 pandemic, including the transmission probability per contact β, the incubation rate α, and the recovery rate γ. According to recent studies of COVID-19 [52,53], we set $\beta = 0.06$, $\alpha = 1/7$ and $\gamma = 1/21$. That said, we set the incubation period to 7 days and the recovery time to 21 days. To start with, we randomly assign a 1 % of the population for communities A and B to the infectious compartment, and initialize the BQ $x(0) = 0$ and the effective intervention policy $\delta(0) = 0$ for all agents. Disregarding the social influence and behavioral response, the contagion dynamics for the densely-connected urban community A and the sparsely-connected rural community B regulated by the conventional SEIR are showcased in Fig. 3: community A reaches a higher peak infection rate with an earlier arrival time. Nonetheless, there is a far cry between the reality and those curves in Fig. 3: ebbs and flows of COVID-19 case count have been reported globally, and multiple resurgent outbreaks are also observed in the U.S.

4.1. Spreading dynamics under different risk perceptions

We set the model parameters on the social layer so as to have immediate cost $c = 0.1$, accumulative factor $a = 0.4$, cost scaling $\varphi = 0.7$, imitation factor $\xi = 0.2$, rational rate $\sigma = 10$, and complying factor $\mu = 50$. We initialize the BQ $x(0) = 0$ for all agents on the social layer, i.e., they are all risk neutral at the onset of infection. We also assume a scaling factor $k = 2$ and risk index $u = 0.5$ for a high level of situational awareness of the infection. In this scenario, the public tends to take risk-averse behaviors in line with the prevalence rate, and the compartment flow dynamics are shown in Fig. 4(a) and (b) for communities A and B, respectively. Compared to the conventional SEIR model, the infectious compartment exhibits oscillatory patterns, and a much lower peak infectious fraction is observed. Conversely, $k = 0.5$ and $u = 4$ are used for a low level of risk awareness. Hence, the public tends to take risky behaviors, resulting in marked increase of the infectious population, as shown in Fig. 4(c) and (d). Numerically, such risky behaviors lead to BQ $x \to -1$ or $\frac{1-x_i(t)}{2} \to 1$ for most agents at the earlier stage of the contagion. According to Eq. (7), our model is approximately equivalent to the conventional SEIR model in this condition, particularly the first 10 time steps before triggering the intervention policy. Next, the non-pharmaceutical intervention is enacted to suppress the spread of contagion. For community A with high population density, the adjustable intervention is not sufficiently intense to contain the disease spread when the public is averse to safeguard measures, which is distinguishable from the infection curves in Figs. 3(a) and 4(c). For community B, the susceptible levels off rapidly after the policy is enacted, which represents a significant departure from the curve in Fig. 3(b).

At the onset of the pandemic, the prevalence $z(t)$ edges up rapidly. When the public possesses high risk aversion (with $k = 2$ and $u = 0.5$), the risk perception η increases at a faster pace than the compliance cost ε_i, promoting risk-averse behaviors (see Eq. (1a)). The imitation of social behaviors further elevates the population BQ, eventually bending the infection curve. The counterbalance between the constituent components of the utility functions is manifested as the spikes on the prevalence curves in Fig. 5(a) and (b). When the public generally ignores the infection risk with $k = 0.5$ and $u = 4$, the compliance cost ε_i dominates the utility function. The behavior imitation further enhances such risk-prone behaviors. Overall, at this extreme risk ignorance, all agents behave without considering the infection, thus the prevalence is fairly similar to the conventional SEIR model without behavioral response (see Fig. 5(c) and (d)). We also note that with high-order interactions between agents, the imitation of social behaviors captures the reinforcement effect. As displayed in Fig. 5(a) and (b), when the population is on high alert, the prevalence rate curves exhibit a lower peak for both communities A and B under the simplicial complex framework compared to the pairwise interaction. At the low risk perception level, the reinforcement of risky responses leads to elevated peaks for communities A and B, though the difference is not substantial as illustrated in Fig. 5(c) and (d).

4.2. The influence of control policy

We conduct another set of simulations to investigate how the control policy in one community affects the other indirectly via the social layer, with 2 levels of intensity, namely, weak $\delta(t) = 0.1$ and strict $\delta(t) = 1.0$ for all time t, instead of the adjustable control policies given in Eqs. (5a) and (5b). Here, we only consider the risk averse scenario. First, we apply a strict control policy to community A and maintain the adjustable policy in line with the prevalence rate for community B. As shown in Fig. 6(a), the bold action against the infection significantly suppresses the prevalence rate for community A, compared to the adjustable policy in Fig. 5(b). Such a strict policy substantially subdues the utility for risky behaviors, thus promoting conservative responses. Simultaneously, agents in community B imitates the behavior of their social contacts, resulting in fluctuation of the prevalence. As time evolves, with the strict government mandate in place, more and more agents adopt the risk-averse responses, and the prevalence in community B also settles at a low level. Next, we impose a strict control policy on community B and maintain the adjustable policy for community A. As shown in Fig. 6(b), the strict policy suppresses the prevalence for community B and agents in community A imitate the protective behaviors in community B to also diminish their prevalence as compared to the scenario of adjustable policies for both communities in Fig. 5(b).

Subsequently, a weak control policy is enacted for one community and an adjustable policy is maintained for another one. As illustrated in Fig. 6(c) and (d), overall, as the population is risk averse, the weak control policy has only a modest impact on agent behaviors and the prevalence of both communities. Compared to Fig. 5(b), the prevalence in community A with weak control policy (see Fig. 6(c)) is slightly

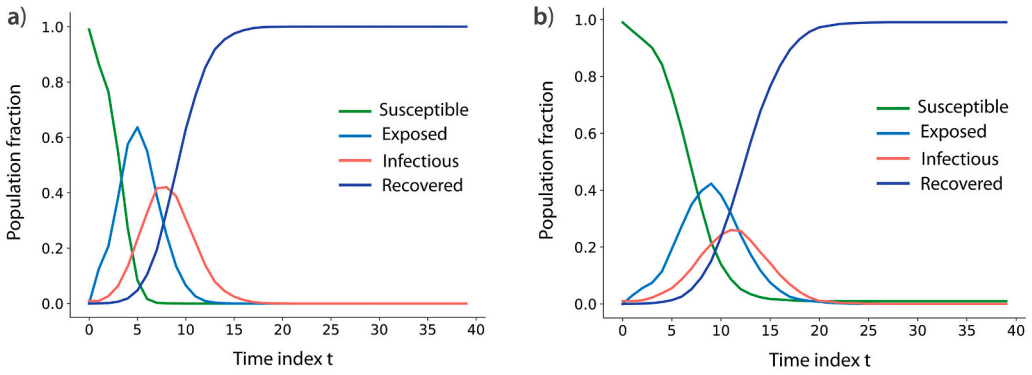

Fig. 3. Population fraction of each compartment under the conventional network SEIR model for (a) communities A and (b) community B, respectively.

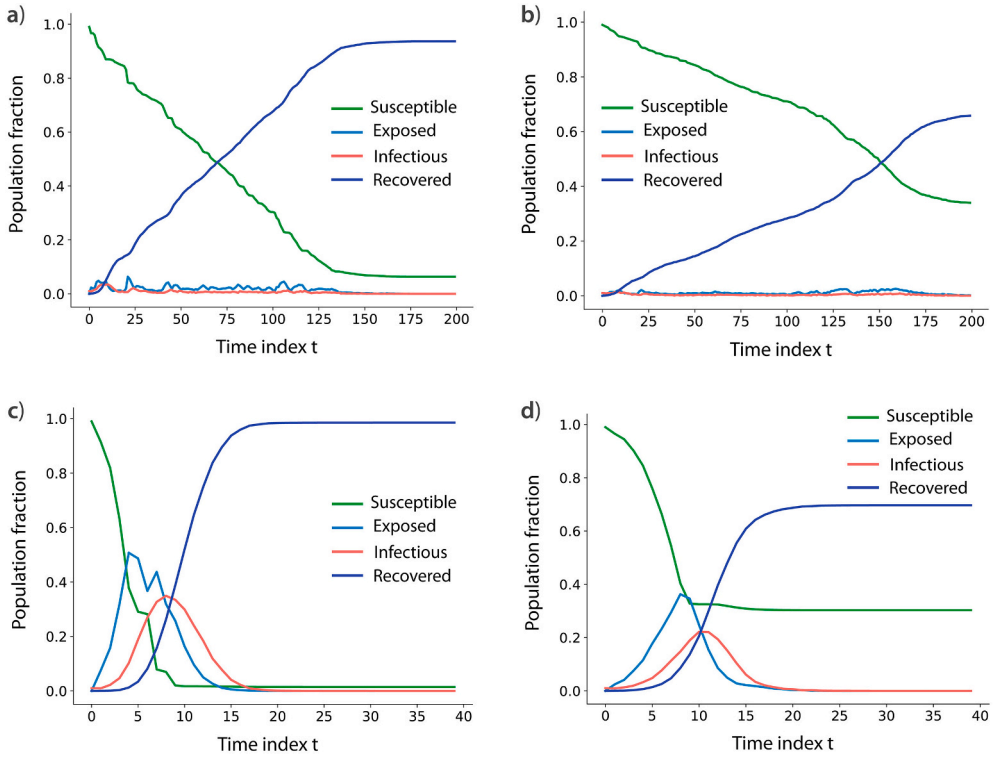

Fig. 4. Population fraction of each compartment under the proposed game-theoretic network SEIR model for (a) community *A* and (b) community *B* with risk-averse behavioral response, and (c) community *A* and (d) community *B* with risk-taking behavioral response.

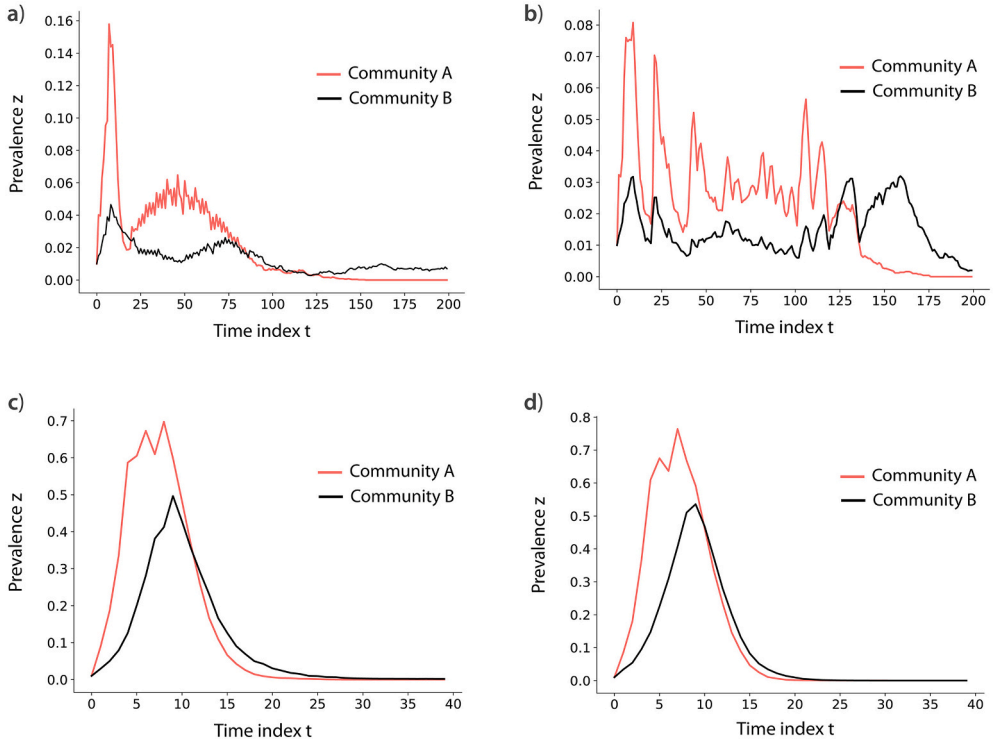

Fig. 5. The prevalence rate $z(t)$ from the game-theoretic network SEIR for the two communities with (a) pairwise and (b) high-order interactions on the social influence layer under risk-averse behavioral response, and with (c) pairwise and (d) high-order interactions on the social influence layer under risk-taking response.

decreased in the first 10 time steps, because the adjustable policy is inactive. Likewise, a weak control policy is also imposed on community *B* leading to a slightly smaller prevalence in community *B*. It is further noted that the strength of the weak control policy ($\delta(t) = 0.1$) is lower than the active adjustable policy ($\delta(t) \geq 0.3$) in community *A* but higher than the inactive adjustable policy ($\delta(t) = 0.0$) in community *B*, as given by the average disease prevalence in both Fig. 6(c) and (d). Therefore, the overall prevalence in community *A* with a weak control policy is

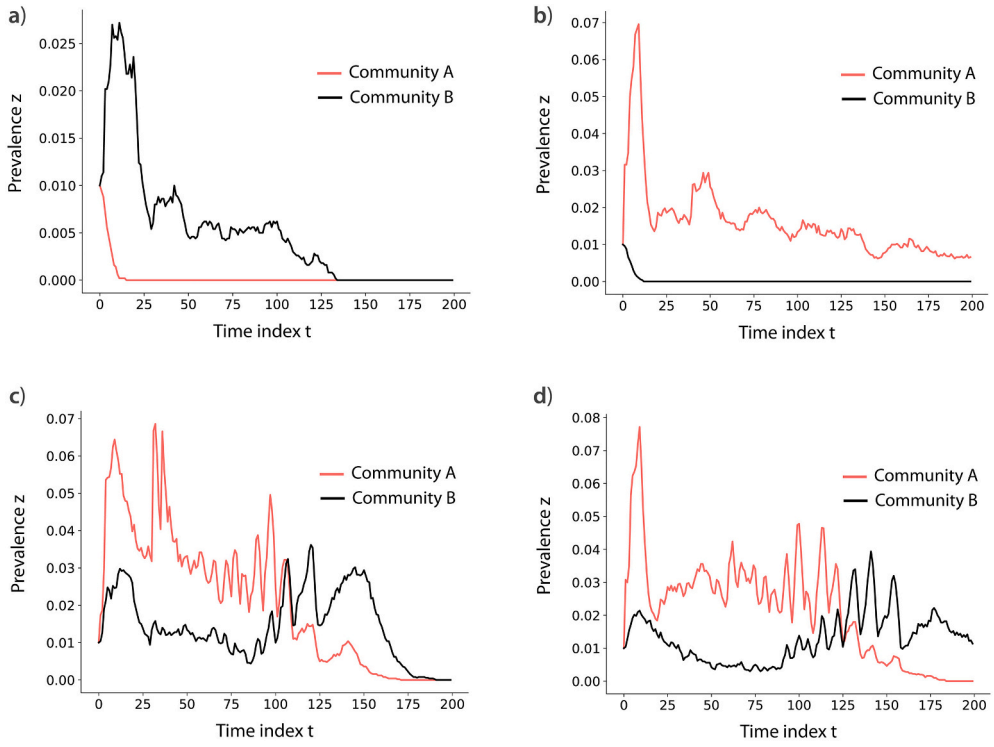

Fig. 6. The prevalence rate $z(t)$ from the game-theoretic network SEIR for the two communities with different levels of control policies: (a) strict control policy $\delta(t) = 1.0$ for community A; (b) strict control policy $\delta(t) = 1.0$ for community B; (c) weak control policy $\delta(t) = 0.1$ for community A; (d) weak control policy $\delta(t) = 0.1$ for community B.

higher than the adjustable policy but the overall prevalence rate in community B with a weak control policy is lower than the adjustable policy.

Based on the results of Fig. 6, we conclude that the control policy for one community can have a significant influence on another community due to the imitation of social behavior ω. Thus, it appears that to reduce the prevalence of the pandemic fast, the best way is to impose a strict control policy on the denser population. Conversely, imposing a strict control policy on a lowly dense population community cannot halt the pandemic fast.

5. Conclusions and discussion

In this study, we build a 3-layer network to inspect the interplay between two isolated physical communities via a common social-influence layer, and articulate the coevolution of behavioral changes of the agents and spreading dynamics of epidemics. A game-theoretic model is developed to capture the coupled behavior-disease dynamics, subject to measures that mimic the impact of government intervention policy, risk perception, compliance cost, and imitation of social contact's behaviors. To avoid a simplistic pairwise interaction formulation, we employ a framework that allows for high-order social interactions in the form of simplicial complexes. Results suggest that the simplicial complex setting for the interaction among the agents enhances the risk-averse or risk-taking behaviors, depending on the contact's response to the social influence (see Fig. 5). Moreover, the conventional SEIR model generally miscalculates the infection case count, since the public may possess different perception on the infection risk and adherence to the government mandate.

Furthermore, as social networks are becoming key avenues for information and opinion formation, particularly during periods of low physical interactions, behavioral adaptation due to social influence has become one critical component to account for in modeling epidemics. This also suggests that policymakers should carefully deal with misinformation and disinformation in a timely manner. Notably, the flareup or resurgent outbreaks of COVID-19 around the world imply that the patchwork intervention policy does not work as anticipated, partially owing to lack of compliance and behavior imitation from social contacts who may reside in a remote community. Thus, coordinated intervention is anticipated to improve the effectiveness of control and mitigation policies. In this sense, our multi-layer network model provides a more sophisticated framework to study this phenomenon, and the insight gleaned therefrom can be adopted to guide policy design for future pandemics, once the model is properly parameterized - which was not an objective of this study. For simplicity, we did not consider human mobility between different physical communities in the current work. As human mobility is regarded as the driving force behind the spatiotemporal dynamics of contagions, we plan to include it in our future investigations. Another mechanistic limitation of this work is that we only adjust the non-pharmaceutical intervention policy in a passive way. In our ongoing work, we will investigate the optimal policy design to prevent contagion resurgence. Such an exercise is needed given that even if extreme government mandates (e.g., complete lockdown) can effectively reduce human contacts and eradicate the infection, they inevitably inflict huge economic and societal costs. Thus, very restricted and static interventions are meant to be implemented only on extreme cases and not for a long duration. An optimal policy design that subdues the future infection load and simultaneously maintains a certain level of social functionalities or human mobility is thus desired.

Data availability statement

The data that support the findings of this study are openly available in Network Repository (NR), reference number [51].

Declaration of competing interest

The authors declare that they have no known competing financial

interests or personal relationships that could have appeared to influence the work reported in this paper.

Data availability

The data that support the findings of this study are openly available in Network Repository (NR), reference number [48].

Acknowledgement

The author CC acknowledges support from the National Science Foundation of the United States (Award Number 2119334, 1927418 and 1927425) and Interdisciplinary Collaborations Grant from Binghamton University. The author YM acknowledges partial support from the Government of Aragon, Spain and "ERDF A way of making Europe" through grant E36-20R (FENOL), from Ministerio de Ciencia e Innovación, Agencia Española de Investigación (MCIN/AEI/10.13039/501100011033) Grant No. PID2020-115800GB-I00, and from Soremartec S.A. and Soremartec Italia, Ferrero Group. The funders have no role in study design, data collection, and analysis, decision to publish, or preparation of the manuscript.

References

[1] Wang D, Small M, Zhao Y. Exploring the optimal network topology for spreading dynamics. Phys A: Stat Mech Appl Feb. 2021;564:125535. https://doi.org/10.1016/j.physa.2020.125535.
[2] Chen Y-C, Lu P-E, Chang C-S, Liu T-H. A time-dependent SIR model for covid-19 with undetectable infected persons. IEEE Trans Netw Sci Eng 2020;7(4):3279–94. https://doi.org/10.1109/TNSE.2020.3024723.
[3] Calafiore GC, Novara C, Possieri C. A modified SIR model for the covid-19 contagion in Italy. In: 2020 59th IEEE conference on decision and control (CDC); 2020. p. 3889–94. https://doi.org/10.1109/CDC42340.2020.9304142.
[4] Cooper I, Mondal A, Antonopoulos CG. A SIR model assumption for the spread of COVID-19 in different communities. Chaos, Solitons Fractals Oct. 2020;139:110057. https://doi.org/10.1016/j.chaos.2020.110057.
[5] Liao Z, Lan P, Liao Z, Zhang Y, Liu S. TW-SIR: time-window based SIR for COVID-19 forecasts. Sci Rep Dec. 2020;10(1):22454. https://doi.org/10.1038/s41598-020-80007-8.
[6] Rizzo A, Frasca M, Porfiri M. Effect of individual behavior on epidemic spreading in activity-driven networks. Phys Rev E Oct. 2014;90(4):042801. https://doi.org/10.1103/PhysRevE.90.042801.
[7] Poletti P, Caprile B, Ajelli M, Pugliese A, Merler S. Spontaneous behavioural changes in response to epidemics. J Theor Biol Sep. 2009;260(1):31–40. https://doi.org/10.1016/j.jtbi.2009.04.029.
[8] Vespignani A. Nat Phys 2012;8(1):1. https://doi.org/10.1038/nphys2160. Jan.
[9] Belykh I, Di Bernardo M, Kurths J, Porfiri M. Evolving dynamical networks. Physica D Jan. 2014;267:1–6. https://doi.org/10.1016/j.physd.2013.10.008.
[10] Perra N, Gonçalves B, Pastor-Satorras R, Vespignani A. Activity driven modeling of time varying networks. Sci Rep 2012;2(1):1. https://doi.org/10.1038/srep00469. Jun.
[11] Ye M, Zino L, Rizzo A, Cao M. Game-theoretic modeling of collective decision making during epidemics. Phys Rev E Aug. 2021;104(2):024314. https://doi.org/10.1103/PhysRevE.104.024314.
[12] Simon HA. Bounded rationality in social science: today and tomorrow. Mind Soc Mar. 2000;1(1):25–39. https://doi.org/10.1007/BF02512227.
[13] K. M. A. Kabir J. Tanimoton.d."Evolutionary game theory modelling to represent the behavioural dynamics of economic shutdowns and shield immunity in the COVID-19 pandemic," R Soc Open Sci vol. 7, no. 9, p. 201095, doi:10.1098/rsos.201095.
[14] Holtz D, et al. Interdependence and the cost of uncoordinated responses to COVID-19. Proc Natl Acad Sci Aug. 2020;117(33):19837–43. https://doi.org/10.1073/pnas.2009522117.
[15] Granell C, Gómez S, Arenas A. Dynamical interplay between awareness and epidemic spreading in multiplex networks. Phys Rev Lett Sep. 2013;111(12):128701. https://doi.org/10.1103/PhysRevLett.111.128701.
[16] Wang Z, Andrews MA, Wu Z-X, Wang L, Bauch CT. Coupled disease–behavior dynamics on complex networks: a review. Phys Life Rev Dec. 2015;15:1–29. https://doi.org/10.1016/j.plrev.2015.07.006.
[17] Iacopini I, Petri G, Barrat A, Latora V. Simplicial models of social contagion. Nat Commun Dec. 2019;10(1):2485. https://doi.org/10.1038/s41467-019-10431-6.
[18] Guilbeault D, Becker J, Centola D. Complex contagions: a decade in review. In: Lehmann S, Ahn Y-Y, editors. Complex spreading phenomena in social systems. Cham: Springer International Publishing; 2018. p. 3–25. https://doi.org/10.1007/978-3-319-77332-2_1.
[19] Wang D, Zhao Y, Leng H, Small M. A social communication model based on simplicial complexes. Phys Lett A Dec. 2020;384(35):126895. https://doi.org/10.1016/j.physleta.2020.126895.
[20] Kermack WO, McKendrick AG, Walker GT. A contribution to the mathematical theory of epidemics. Proceedings of the Royal Society of London. Series A, Containing Papers of a Mathematical and Physical Character 1927;115(772):700–21. https://doi.org/10.1098/rspa.1927.0118.
[21] Chen S, Li Q, Gao S, Kang Y, Shi X. State-specific projection of COVID-19 infection in the United States and evaluation of three major control measures. Sci Rep 2020;10(1):1. https://doi.org/10.1038/s41598-020-80044-3. Dec.
[22] Thomas LJ, et al. Spatial heterogeneity can lead to substantial local variations in COVID-19 timing and severity. Proc Natl Acad Sci Sep. 2020;117(39):24180–7. https://doi.org/10.1073/pnas.2011656117.
[23] Adhikari S, Pantaleo NP, Feldman JM, Ogedegbe O, Thorpe L, Troxel AB. Assessment of community-level disparities in coronavirus disease 2019 (COVID-19) infections and deaths in large US metropolitan areas. JAMA Netw Open Jul. 2020;3(7):e2016938. https://doi.org/10.1001/jamanetworkopen.2020.16938.
[24] Prem K, et al. The effect of control strategies to reduce social mixing on outcomes of the COVID-19 epidemic in Wuhan, China: a modelling study. Lancet Public Health 2020;5(5):e261–70. https://doi.org/10.1016/S2468-2667(20)30073-6.
[25] Kucharski AJ, et al. Early dynamics of transmission and control of COVID-19: a mathematical modelling study. Lancet Infect Dis May 2020;20(5):553–8. https://doi.org/10.1016/S1473-3099(20)30144-4.
[26] Tran-Thi C-G, Choisy M, Daniel Zucker J. Quantifying the effect of synchrony on the persistence of infectious diseases in a metapopulation. In: 2016 IEEE RIVF international conference on computing communication technologies, research, innovation, and vision for the future (RIVF); 2016. p. 229–34. https://doi.org/10.1109/RIVF.2016.7800299.
[27] Venkatramanan S, et al. Spatio-temporal optimization of seasonal vaccination using a metapopulation model of influenza. IEEE International Conference on Healthcare Informatics (ICHI) 2017;2017:134–43. https://doi.org/10.1109/ICHI.2017.83.
[28] Brockmann D, Helbing D. The hidden geometry of complex, network-driven contagion phenomena. Science Dec. 2013;342(6164):1337–42. https://doi.org/10.1126/science.1245200.
[29] Rădulescu A, Williams C, Cavanagh K. Management strategies in a SEIR-type model of COVID 19 community spread. Sci Rep Dec. 2020;10(1):21256. https://doi.org/10.1038/s41598-020-77628-4.
[30] Weitz JS, Park SW, Eksin C, Dushoff J. Awareness-driven behavior changes can shift the shape of epidemics away from peaks and toward plateaus, shoulders, and oscillations. Proc Natl Acad Sci U S A Dec. 2020;117(51):32764–71. https://doi.org/10.1073/pnas.2009911117.
[31] Johnston MD, Pell B. A dynamical framework for modeling fear of infection and frustration with social distancing in COVID-19 spread. MBE 2020;17(6):mbe-17-06-401. https://doi.org/10.3934/mbe.2020401.
[32] Scabini LFS, Ribas LC, Neiva MB, Junior AGB, Farfán AJF, Bruno OM. Social interaction layers in complex networks for the dynamical epidemic modeling of COVID-19 in Brazil. Phys A: Stat Mech Appl Feb. 2021;564:125498. https://doi.org/10.1016/j.physa.2020.125498.
[33] Chinazzi M, et al. The effect of travel restrictions on the spread of the 2019 novel coronavirus (COVID-19) outbreak. Science Apr. 2020;368(6489):395–400. https://doi.org/10.1126/science.aba9757.
[34] Wu JT, Leung K, Leung GM. Nowcasting and forecasting the potential domestic and international spread of the 2019-nCoV outbreak originating in Wuhan, China: a modelling study. Lancet Feb. 2020;395(10225):689–97. https://doi.org/10.1016/S0140-6736(20)30260-9.
[35] Cui Y, Ni S, Shen S. A network-based model to explore the role of testing in the epidemiological control of the COVID-19 pandemic. BMC Infect Dis Dec. 2021;21(1):58. https://doi.org/10.1186/s12879-020-05750-9.
[36] Albert R, Barabási A-L. Statistical mechanics of complex networks. Rev Mod Phys Jan. 2002;74(1):47–97. https://doi.org/10.1103/RevModPhys.74.47.
[37] Chang S, et al. Mobility network models of COVID-19 explain inequities and inform reopening. Nature 2021;589(7840):7840. https://doi.org/10.1038/s41586-020-2923-3. Jan.
[38] Meloni S, Perra N, Arenas A, Gómez S, Moreno Y, Vespignani A. Modeling human mobility responses to the large-scale spreading of infectious diseases. Sci Rep 2011;1(1):1. https://doi.org/10.1038/srep00062. Aug.
[39] Alvarez-Zuzek LG, Rocca CEL, Iglesias JR, Braunstein LA. Epidemic spreading in multiplex networks influenced by opinion exchanges on vaccination. PLOS ONE Nov. 2017;12(11):e0186492. https://doi.org/10.1371/journal.pone.0186492.
[40] Granell C, Gómez S, Arenas A. Competing spreading processes on multiplex networks: awareness and epidemics. Phys Rev E Jul. 2014;90(1):012808. https://doi.org/10.1103/PhysRevE.90.012808.
[41] Massaro E, Bagnoli F. Epidemic spreading and risk perception in multiplex networks: a self-organized percolation method. Phys Rev E Nov. 2014;90(5):052817. https://doi.org/10.1103/PhysRevE.90.052817.
[42] Buono C, Alvarez-Zuzek LG, Macri PA, Braunstein LA. Epidemics in partially overlapped multiplex networks. PLOS ONE Mar. 2014;9(3):e92200. https://doi.org/10.1371/journal.pone.0092200.
[43] da Silva PCV, Velásquez-Rojas F, Connaughton C, Vazquez F, Moreno Y, Rodrigues FA. Epidemic spreading with awareness and different timescales in multiplex networks. Phys Rev E Sep. 2019;100(3):032313. https://doi.org/10.1103/PhysRevE.100.032313.
[44] Wang Z, Xia C, Chen Z, Chen G. Epidemic propagation with positive and negative preventive information in multiplex networks. IEEE Trans Cyber Mar. 2021;51(3):1454–62. https://doi.org/10.1109/TCYB.2019.2960605.
[45] Nicola M, et al. The socio-economic implications of the coronavirus pandemic (COVID-19): a review. Int J Surg Jun. 2020;78:185–93. https://doi.org/10.1016/j.ijsu.2020.04.018.

[46] Flaxman S, et al. Estimating the effects of non-pharmaceutical interventions on COVID-19 in Europe. Nature 2020;584(7820):7820. https://doi.org/10.1038/s41586-020-2405-7. Aug.
[47] Aleta A, Moreno Y. Evaluation of the potential incidence of COVID-19 and effectiveness of containment measures in Spain: a data-driven approach. BMC Med Dec. 2020;18(1):157. https://doi.org/10.1186/s12916-020-01619-5.
[48] Ventura PC, Aleta A, Rodrigues FA, Moreno Y. Modeling the effects of social distancing on the large-scale spreading of diseases. Epidemics Mar. 2022;38:100544. https://doi.org/10.1016/j.epidem.2022.100544.
[49] N. Masuda J. C. Miller P. Holme n.d. "Concurrency measures in the era of temporal network epidemiology: a review," J. R. Soc. Interface, vol. 18, no. 179, p. 20210019, doi:10.1098/rsif.2021.0019.
[50] McMahan CS, et al. COVID-19 wastewater epidemiology: a model to estimate infected populations. Lancet Planet Health Dec. 2021;5(12):e874–81. https://doi.org/10.1016/S2542-5196(21)00230-8.
[51] Rossi RA, Ahmed NK. The network data repository with interactive graph analytics and visualization. In: 29th AAAI conference on artificial intelligence; 2015. p. 4292–3. Jan.
[52] Moghadas SM, et al. The implications of silent transmission for the control of COVID-19 outbreaks. Proc Natl Acad Sci U S A Jul. 2020;117(30):17513–5. https://doi.org/10.1073/pnas.2008373117.
[53] Hou C, et al. The effectiveness of quarantine of Wuhan city against the Corona virus disease 2019 (COVID-19): a well-mixed SEIR model analysis. J Med Virol Jul. 2020;92(7):841–8. https://doi.org/10.1002/jmv.25827.